



## LJMU Research Online

**Graef, F, Vukosavljevic, B, Michel, J-P, Wirth, M, Ries, O, De Rossi, C, Windbergs, M, Rosilio, V, Ducho, C, Gordon, S and Lehr, C-M**

**The bacterial cell envelope as delimiter of anti-infective bioavailability - An in vitro permeation model of the Gram-negative bacterial inner membrane.**

<http://researchonline.ljmu.ac.uk/id/eprint/6677/>

### Article

**Citation** (please note it is advisable to refer to the publisher's version if you intend to cite from this work)

**Graef, F, Vukosavljevic, B, Michel, J-P, Wirth, M, Ries, O, De Rossi, C, Windbergs, M, Rosilio, V, Ducho, C, Gordon, S and Lehr, C-M (2016) The bacterial cell envelope as delimiter of anti-infective bioavailability - An in vitro permeation model of the Gram-negative bacterial inner membrane.**

LJMU has developed [LJMU Research Online](#) for users to access the research output of the University more effectively. Copyright © and Moral Rights for the papers on this site are retained by the individual authors and/or other copyright owners. Users may download and/or print one copy of any article(s) in LJMU Research Online to facilitate their private study or for non-commercial research. You may not engage in further distribution of the material or use it for any profit-making activities or any commercial gain.

The version presented here may differ from the published version or from the version of the record. Please see the repository URL above for details on accessing the published version and note that access may require a subscription.

For more information please contact [researchonline@ljmu.ac.uk](mailto:researchonline@ljmu.ac.uk)

<http://researchonline.ljmu.ac.uk/>

## Supplementary Material

### The Bacterial Cell Envelope as Delimiter of Anti-Infective Bioavailability – An *In Vitro* Permeation Model of the Gram-Negative Bacterial Inner Membrane

Florian Graef<sup>a</sup>, Branko Vukosavljevic<sup>a</sup>, Jean-Philippe Michel<sup>b</sup>, Marius Wirth<sup>c</sup>, Oliver Ries<sup>c</sup>, Chiara De Rossi<sup>a</sup>, Maïke Windbergs<sup>a</sup>, Véronique Rosilio<sup>b</sup>, Christian Ducho<sup>c</sup>, Sarah Gordon<sup>a\*</sup> and Claus-Michael Lehr<sup>a,d\*</sup>

<sup>a</sup> Helmholtz Institute for Pharmaceutical Research Saarland (HIPS), Helmholtz Center for Infection Research (HZI), Department of Drug Delivery, Campus E8 1, 66123 Saarbrücken, Germany

E-mail: Florian.Graef@helmholtz-hzi.de, Branko.Vukosavljevic@helmholtz-hzi.de, Maïke.Windbergs@helmholtz-hzi.de, Chiara.DeRossi@helmholtz-hzi.de, Sarah.Gordon@helmholtz-hzi.de, Claus-Michael.Lehr@helmholtz-hzi.de

<sup>b</sup> Institut Galien Paris Sud, UMR 8612, Univ Paris-Sud, CNRS, Université Paris-Saclay, 5 rue J.B. Clément, F-92290 Châtenay-Malabry, France

E-Mail: jean-philippe.michel@u-psud.fr, veronique.rosilio@u-psud.fr

<sup>c</sup> Saarland University, Department of Pharmacy, Pharmaceutical and Medicinal Chemistry, Campus C2 3, 66123 Saarbrücken, Germany

E-Mail: marius.wirth@uni-saarland.de, christian.ducho@uni-saarland.de

<sup>d</sup> Saarland University, Department of Pharmacy, Biopharmacy and Pharmaceutical Technology, Campus E8 1, 66123 Saarbrücken, Germany

\* Corresponding authors

**Table S1** . Key physicochemical parameters and characteristics of fluorescent dyes used for permeability investigations, as well as parameters utilized for compound quantification.

Fluorescent dye	logD <sub>(pH 7.4)</sub> <sup>a)</sup>	M <sub>w</sub> (g/mol)	PSA (Å <sup>2</sup> ) <sup>b)</sup>	H-bond donors/acceptors <sup>b)</sup>	Initial donor concentration (μM)	λ <sub>exc</sub> (nm) – λ <sub>em</sub> (nm)
Calcein	-1.46	622.5	232	6 / 5	22	470 - 530
Fluorescein	-0.43	376.2	76	2 / 5	26.6	485 - 530
Rhodamine 123	1.17	344.4	85.4	3 / 5	14.4	540 - 580
Rhodamine B	1.96	479	52.8	1 / 5	130.4	540 - 600
Rhodamine B isothiocyanate	2.03	536	86.5	1 / 7	116.6	540 - 600

<sup>a)</sup> Values determined by the shake flask method (according to OECD guideline for the testing of chemicals section 1: physical-chemical properties, test 107)

<sup>b)</sup> Values taken from Pubchem

PSA: polar surface area

35 **Table S2.** Transport study and quantification parameters of employed  $\beta$ -blockers and  
 36 antibiotics. Concentrations of  $\beta$ -blockers and antibiotics initially added to the apical  
 37 compartment of IM or mammalian comparator model-coated Transwell<sup>®</sup> filter inserts for  
 38 permeability investigations, together with drug quantification parameters.  
 39

Compound	Initial donor concentration (mM)	$\lambda_{\max}$ (nm)	Binary solvent system (A:B)	Flow rate (ml min <sup>-1</sup> )	Retention time (min)
Atenolol	3.6	280	90:10	0.2	2.4
Metoprolol	16.4	280	70:30	0.4	1.1
Timolol	7.8	280	80:20	0.4	1.7
Nadolol	5.7	280	85:15	0.2	3.1
Acebutolol	0.89	235	70:30	0.2	2.2
Alprenolol	4	270	65:35	0.4	1.4
Ciprofloxacin	0.06	280	77:23	0.2	3.6
Minocycline	2.19	270	80:20	0.2	4.2

40  
41  
42  
43  
44  
45  
46  
47  
48  
49  
50  
51  
52  
53  
54  
55  
56  
57  
58  
59  
60  
61  
62  
63  
64  
65  
66  
67  
68  
69  
70  
71  
72  
73  
74

**Table S3.** Size and surface charge of bacteria- and mammal-specific liposomes. Z-average (nm) and surface charge ( $\zeta$ -potential, mV) of POPE:POPG:CL (bacteria-specific) and PC (mammal-specific) liposomes. Values represent mean  $\pm$  SEM from 4 batches, each measured in triplicate.

Liposome Formulation	z-average (nm)	$\zeta$ -potential (mV)
<b>POPE:POPG:CL</b>	413.5 $\pm$ 13.7	-31.3 $\pm$ 1.4
<b>PC</b>	665.8 $\pm$ 30.4	-4.9 $\pm$ 0.3

75 **Analysis of surface pressure isotherms**

76

77 The area occupied by phospholipid (PL) molecules in the bacterial PL mixed monolayer, at  
78 each surface pressure ( $\pi$ ), were calculated according to the additivity rule as shown in  
79 equation S1:

80

$$81 [A_{TH}]_{\pi} = [X_{POPE} A_{POPE} + X_{POPG} A_{POPG} + X_{CL} A_{CL}]_{\pi} \quad (S1)$$

82

83 where  $[A_{TH}]_{\pi}$  is the theoretical molecular area, X is the PL molar fraction and A is the PL  
84 molecular area in the pure PL monolayer.

85

86 The excess molecular areas  $\Delta A^{EXC}$  were then calculated from the difference between the  
87 theoretical and experimental ( $A_M$ ) molecular area values:  $A_M - A_{TH}$ . Negative deviations from  
88 the additivity rule indicate area condensation and may imply intermolecular accommodation  
89 and/or dehydration interactions between lipids in the mixed films; positive deviations from  
90 the additivity rule are the result of area expansion and would account for unfavorable  
91 interactions between the different components leading to poor mixing [1].

92 The free energy of mixing  $\Delta G^M$  was calculated according to the Equation S2 [2]:

93

$$94 \Delta G^M = \Delta G^{EXC} + \Delta G^{IDEAL} \quad (S2)$$

95

96 where  $\Delta G^{EXC}$  is the excess free energy (shown in equation S3) and  $\Delta G^{IDEAL}$  the free energy of  
97 mixing (shown in equation S4) for an ideal mixture.

98

$$100 \Delta G^{EXC} = \int_0^{\pi} \Delta A^{EXC} d\pi \quad (S3)$$

101

$$102 \Delta G^{IDEAL} = RT (X_{POPE} \ln X_{POPE} + X_{POPG} \ln X_{POPG} + X_{CL} \ln X_{CL}) \quad (S4)$$

103

104

105 with R the universal gas constant and T the absolute temperature.

106

107

108

109

110

111

112

113

114

115

116

117

118

119

120

121

122

123

124

125

126  
 127  
 128  
 129  
 130  
 131  
 132  
 133  
 134  
 135  
 136  
 137  
 138  
 139  
 140  
 141  
 142  
 143  
 144  
 145  
 146  
 147  
 148  
 149  
 150  
 151  
 152  
 153  
 154  
 155  
 156  
 157  
 158  
 159  
 160  
 161  
 162  
 163  
 164  
 165  
 166  
 167  
 168  
 169  
 170  
 171  
 172  
 173  
 174  
 175  
 176

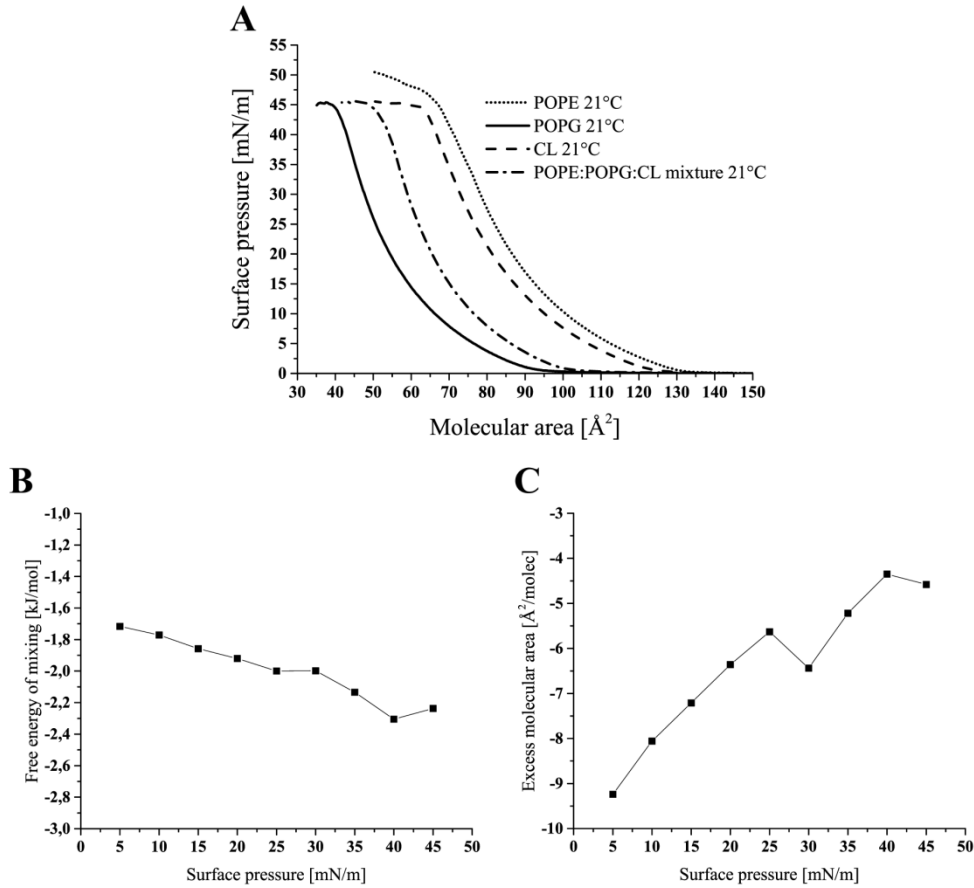


**Fig. S1.** Langmuir studies of pure bacteria-relevant PLs and physiological mixture. Comparison of the isotherms for the pure bacteria-relevant PLs and the inner membrane (IM) relevant mixture (A), together with the free energy of mixing ( $\Delta G^M$ ) (B) and the excess molecular area ( $\Delta A^{\text{EXC}}$ ) (C) with respect to surface pressure of the ternary PL blend. The occurrence of negative excess molecular area and free energies account for a good miscibility of the components of the ternary blend at all studied surface pressures, indicating an appropriate PL mixture.

177 **Electrical resistance measurements**

178

179 Simulated transport experiments were performed by exposing the IM model to Krebs-Ringer  
180 buffer (KRB; adjusted to pH 7.4). Resistance ( $R$ ;  $\Omega$ ) was subsequently measured over 5 h,  
181 using a handheld chopstick electrode (STX-2) and an epithelial voltohmmeter (EVOM, World  
182 Precision Instruments, Berlin, Germany). Cell culture plates containing models coated onto  
183 Transwell<sup>®</sup> filter inserts were placed on an orbital shaker (IKA<sup>®</sup>-Werke GmbH and Co KG,  
184 Staufen, Germany) set at 150 rpm and kept in an incubator at 37 °C between the  
185 measurements. The electrical resistance (ER) provided by each model membrane at each  
186 measured time point was calculated via equation S5:

187

188 
$$ER (\Omega * cm^2) = (R_{\text{insert with model membrane}} / R_{\text{blank insert}}) * 1.12 \text{ cm}^2 \tag{S5}$$

189

190

191 where 1.12 cm<sup>2</sup> represents the surface area of the Transwell<sup>®</sup> filter insert.

192

193 ER as such constitutes a parameter which provides an indication of barrier properties, with a  
194 resistance value of 400  $\Omega \text{ cm}^2$  often being considered as an accepted minimum value in live  
195 cell-based models [3,4].

196

197

198

199

200

201

202

203

204

205

206

207

208

209

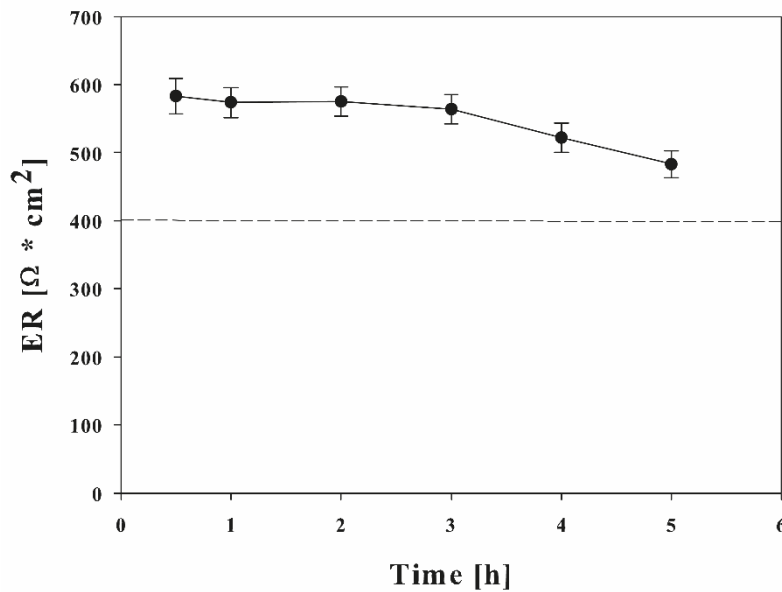
210

211

212

213

214



215 **Fig. S2.** Blank corrected ER values of the bacterial IM model. The high and relatively  
216 constant ER profile indicates sufficient model barrier properties. The dashed line indicates the  
217 accepted minimum ER level of live cell-based models such as Caco-2 cell monolayers, for  
218 reference. Values represent mean  $\pm$  SEM; n=6 from 2 individual experiments.

219

220

221

222

223

224

225

226

227

228 **Optical topography evaluation of IM and mammalian comparator model surfaces**

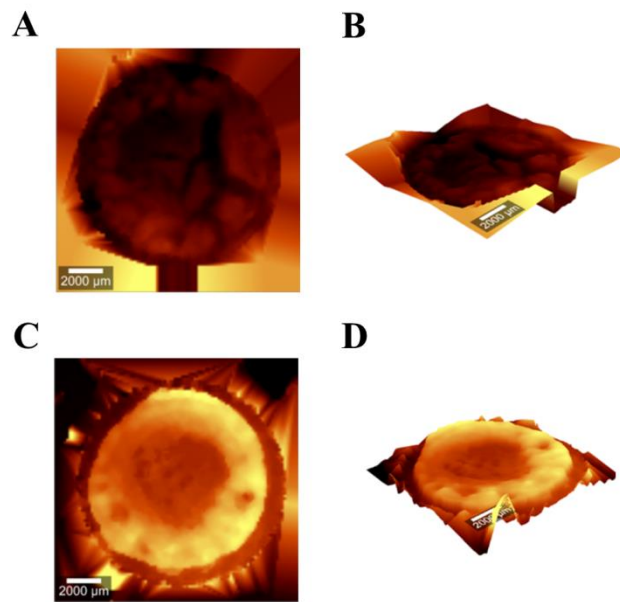
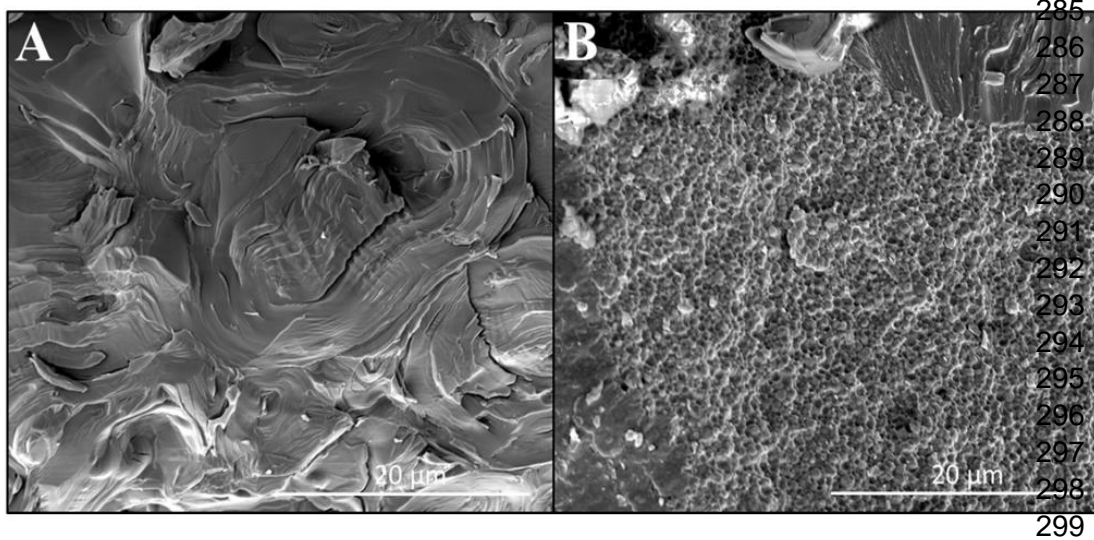


**Fig. S3.** Optical topography profiles of the overall model surfaces. Two- and three-dimensional optical topography profiles of the overall model surface area in case of the IM (A, B) as well as the mammalian comparator model (C, D).

279 **Cryogenic scanning electron microscopy (cryo-SEM) evaluation**

280

281 Both IM and mammalian comparator models were frozen in liquid nitrogen to conserve the  
282 inner morphology followed by the preparation of cross-sections. Samples were further cryo-  
283 coated using a fracture coater (MED 020, Leica microsystems GmbH, Wetzlar, Germany) and  
284 subsequently imaged using a Quanta™ FEG 3 D SEM (FEI, Hillsboro, Oregon, USA).



300 **Fig. S4.** Inner morphology assessment via cryo-SEM. Cryo-SEM cross section images of the  
301 bacterial IM (A) and mammalian comparator model (B) indicating differences in inner  
302 morphology as a result of the different lipid composition.

303

304

305

306

307

308

309

310

311

312

313

314

315

316

317

318

319

320

321

322

323

324

325

326

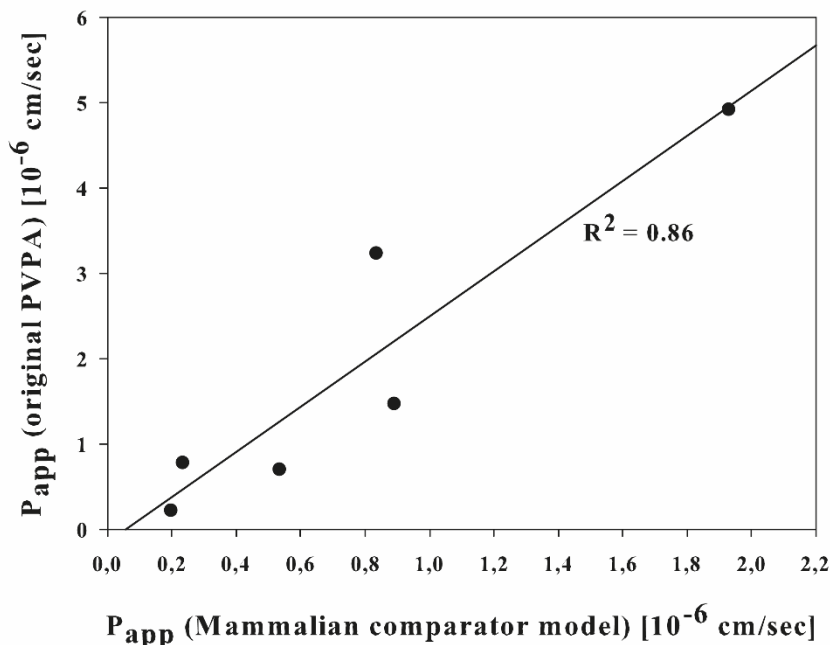
327

328

329

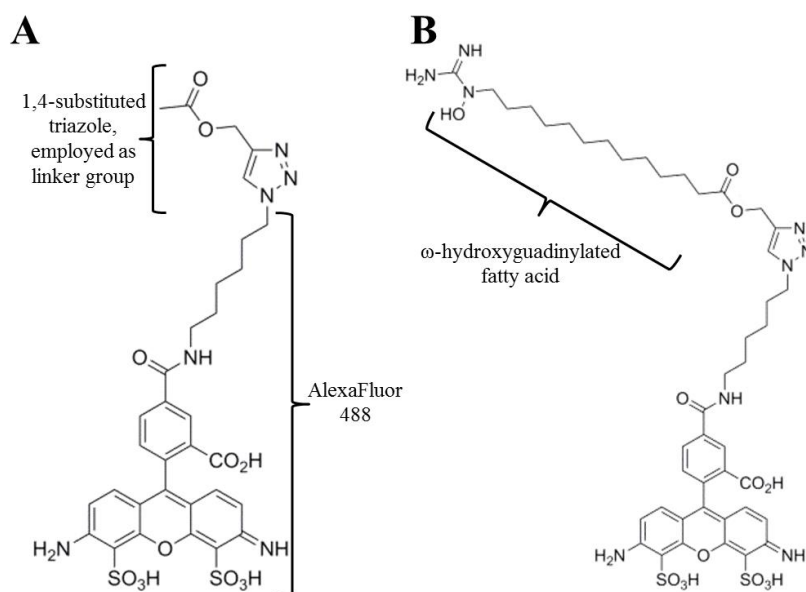


330 Comparison of  $\beta$ -blocker apparent permeability coefficient ( $P_{app}$ ) values of the original  
331 phospholipid-vesicle based permeation assay (PVPA) and the mammalian comparator  
332 model (both prepared using PC as a mammal-relevant lipid)  
333  
334  
335



355 **Fig. S5.** Comparison of  $\beta$ -blocker  $P_{app}$  values in the current mammalian comparator model  
356 (abscissa) with corresponding  $P_{app}$  values of the same compounds in the original human  
357 intestinal-mimicking PVPA (ordinate). A considerable correlation between  $P_{app}$  data obtained  
358 in the two models is indicated, confirming that the current mammalian comparator model  
359 provides relevant and acceptable mammal-specific permeation information.  
360  
361  
362  
363  
364  
365  
366  
367  
368  
369  
370  
371  
372  
373  
374  
375  
376  
377  
378  
379

380 Structures of fluorescently labeled muraymycin A-derived functionalized fatty acid and  
381 reference compound:  
382  
383



405 **Fig. S6.** Anti-infective derived structures utilized for permeability investigations.. Employed  
406 reference compound composed of the fluorescent label (AlexaFluor 488) and the linker group  
407 (A), as well as the fluorescently labeled  $\omega$ -hydroxyguanidinylated fatty acid moiety, which  
408 were employed to demonstrate the validity of the IM model as well as emphasize its  
409 advantages in comparison to an existing *in vitro* bacterial permeation model. The model  
410 conjugate of the  $\omega$ -hydroxyguanidinylated fatty acid has been conceived based on the  
411 structure of the naturally occurring nucleoside antibiotic muraymycin A1 [5].  
412  
413

414 **References**

- 415 [1] F. Müller-Landau, D.A. Cadenhead, B.M.J. Kellner, The nature of the liquid  
416 expanded/liquid condensed phase change in insoluble monolayers at the air/water interface, *J.*  
417 *Colloid Interface Sci.*, 73 (1980) 264-266.  
418 [2] T.-H. Chou, I.M. Chu, C.-H. Chang, Interaction of paclitaxel with DSPC in monolayers at  
419 the air/water interface at different temperatures, *Colloids Surf., B*, 25 (2002) 147-155.  
420 [3] F. Leonard, E.M. Collnot, C.M. Lehr, A three-dimensional coculture of enterocytes,  
421 monocytes and dendritic cells to model inflamed intestinal mucosa *in vitro*, *Mol. Pharm.*, 7  
422 (2010) 2103-2119.  
423 [4] C.I. Grainger, L.L. Greenwell, D.J. Lockley, G.P. Martin, B. Forbes, Culture of Calu-3  
424 cells at the air interface provides a representative model of the airway epithelial barrier,  
425 *Pharm. Res.*, 23 (2006) 1482-1490.  
426 [5] L.A. McDonald, L.R. Barbieri, G.T. Carter, E. Lenoy, J. Lotvin, P.J. Petersen, M.M.  
427 Siegel, G. Singh, R.T. Williamson, Structures of the muraymycins, novel peptidoglycan  
428 biosynthesis inhibitors, *J. Am. Chem. Soc.*, 124 (2002) 10260-10261.